Protection of 18th century paper using antimicrobial nano-magnesium oxide

Isabel Franco Castillo,[1†] Laura De Matteis,[2*†] Clara Marquina,[1,3] Esther García Guillén[4], Jesús Martínez de la Fuente,[1] Scott G. Mitchell[1*]

1. Instituto de Ciencia de Materiales de Aragón (ICMA), Consejo Superior de Investigaciones Científicas (CSIC)-Universidad de Zaragoza and CIBER-BBN, C/ Pedro Cerbuna 12, 50009 Zaragoza (Spain).

2. Instituto de Nanociencia de Aragón (INA), Universidad de Zaragoza and CIBER-BBN, C/ Mariano Esquillor s/n, 50018 Zaragoza (Spain).

3. Departamento de Física de la Materia Condensada, Universidad de Zaragoza, C/ Pedro Cerbuna 12, 50009 Zaragoza (Spain).

4. Real Jardín Botánico, Consejo Superior de Investigaciones Científicas (CSIC), Madrid (Spain).

† These authors contributed equally

* E-mail: lauradem@unizar.es and scott@unizar.es

Abstract

Magnesium oxide nanoparticles (MgO NPs) have attracted considerable interest as antimicrobial agents in a wide variety of applications. We report a simple synthetic route towards MgO NPs (average diameter 10 nm) possessing potent antibacterial activity against both Gram-negative and Gram-positive bacteria. Detailed electron microscopy studies show how these particles induce oxidative stress, cell membrane leakage and cell death in bacteria at low NP concentrations, but remain non-toxic to eukaryotic cells. Applying a homogeneous dispersion of these nanoparticles on 18th century paper proved to be a highly effective means of preventing bacterial colonisation without altering the appearance of the paper samples, thus opening the doors to the use of these colourless, low-cost, and scalable nanoparticles for preventing biodeterioration in a range of paper-based objects and surfaces.

Keywords: magnesium oxide**,** nanoparticles, paper heritage, antimicrobial activity, oxidative stress.

1. Introduction

The enduring threat of microbial contamination to historical and contemporary objects of art in archives and in museums remains to be one of the principal problems of cultural heritage conservation. Microbes can penetrate deep within the microstructures of materials causing material loss from acid corrosion, enzymatic degradation and mechanical attack, all of which induce esthetical spoiling of paintings, sculptures, textiles, ceramics, metals, books and manuscripts alike (Sterflinger et al., 2014). Regular decontamination of infected artefacts, exhibition areas and storage rooms/depots results in significant expenditures for museums, local authorities and private collectors. Ultimately, material loss brought about by prolonged microbial attack can result in loss of the cultural and historical value of paintings, books and manuscripts – the socioeconomic cost of which is inestimable (Sterflinger et al., 2012; La Russa 2014). Furthermore, microbial contamination in libraries, museums and their storage rooms/depots can also represent a serious threat to the health and occupational safety of restorers, museum personnel and the general public (Skóra et al., 2015).

Metal oxide nanoparticles for example ZnO, MgO, CuO and CaO are being studied as novel inorganic antimicrobial agents for potential applications in food, the environment and healthcare (Hajipour et al., 2012; Dizaj et al., 2014). Nanostructured inorganic materials possess unique tuneable physicochemical properties and, moreover, the combination of their large surface area and dimensions allows them to interact and internalise within cells, respectively, meaning that they display a broad spectrum of antibacterial activity. Moreover, their modular nature means that a library of relatively low cost materials with different sizes, shapes, surface properties, and chemical compositions can be developed leading to a great potential for developing effective antimicrobial agents with high stability under harsh environmental conditions. Despite the advance of this field of research in recent years, the antibacterial mechanism of action of metal oxide nanoparticles is in most cases not entirely understood. Magnesium oxide nanoparticles (MgO NPs) have received significant attention as antibacterial agents in recent years due to their high stability and low cost based on their preparation from economical precursors (He et al., 2016; Tang et al. 2012). The mechanism of antibacterial activity of MgO NPs has been attributed to the production of reactive oxygen species (ROS), which induce oxidative stress and lipid peroxidation in bacteria (Tang et al., 2014) as well as non-ROS mediated bacterial toxicity mechanisms (Leung et al., 2014). It is important to note that the antibacterial effect is often species and genus dependent and depends upon the size, shape, chemical composition and surface properties (e.g. hydrophobicity) of the nanoparticles (Raghupathi et al., 2011; Hajipour et al., 2012).

Although MgO NPs are generally regarded as safe (Ge et al., 2011), the application of any antibacterial nanomaterial and its nanotoxicological profile is a major concern. Currently, MgO NPs are used as additives in heavy fuel-oil (Park et al., 2006), for the cleaning of fuel-oil pipelines, avoidance of sludge formation in storage tanks and protection of boilers against corrosion. MgO has been used as a mineral supplement source for magnesium, an essential nutrient for the human body (Srinivasan et al., 2017) and they are also used for diverse applications in medicine, e.g. for the relief of cardiovascular disease and stomach problems and as anti-cancer therapy (Krishnamoorthy et al., 2012). As already mentioned, toxic effects are highly dependent on the physicochemical properties of each individual nanoparticle as well as on the types of cells tested (Reddy et al., 2007). It therefore follows that an extensive evaluation of nanoparticles on different biological systems is needed to determine their toxicity. As an illustration, despite the aforementioned examples showing the low cytotoxicity of MgO NPs, they have been shown to display toxicity on early developmental and larval stages of zebrafish (Ghobadian et al., 2015). One of the great challenges of nanotechnology is the corresponding environmental health and safety implications of the widespread use of nanomaterials, since the properties of engineered nanomaterials are potentially highly hazardous to the human population due to their potential for high ecotoxicity. The widespread use of nanoparticles and their inevitable release into the general environment ultimately means that they will find their way into terrestrial, aquatic and atmospheric environments where their toxicity, behaviour and ultimate fate are largely unknown (Bondarenko et al., 2013).

Recently, there has been a drive for greater use of nanomaterials in the conservation of cultural heritage (Baglioni et al., 2015, La Russa et al., 2012 and 2016). Recent examples include their use for protecting stone monuments (Sierra-Fernandez et al., 2017a), textiles (Pietrzak et al., 2017), murals (Baglioni et al., 2012), glass (Shirakawa et al., 2016) and paper (Asghar Ariafar et al., 2017). Both silver (Koizhaiganova 2015) and nano-silver (Li et al., 2017) are studied frequently and some studies have even thoroughly evaluated the sensitivity of museum microbes to nanosilver (Gutarowska et al., 2012), but cheaper more readily available metal-

oxide particles have been shown to serve as alternative solutions to biodeterioration issues (Ruffolo S. A., et al., 2010 and Sierra-Fernandez et al., 2017b).

The aim of the research presented herein was to study the use of nano-magnesium oxide particles to protect a variety of 18th century papers from the Archives of the Real Jardín Botánico in Madrid (Spain) from microbial contamination. These papers have been selected as a representative sample of different paper qualities that were used as herbarium materials at the end of the 18th century to keep plant specimens (herbarium sheets) dried for other purposes. They are part of the old herbarium paper sheets kept in the RJB archive before plants were stored with standardized herbarium paper sheets (c. 1980). They arrived at the RJB between 1785 and 1800 and have been kept here since, in a rather dry environment, but without further specific preserving measures (controlled humidity and temperature). Furthermore, we wished to demonstrate how a combination of antibacterial assays (solution-based quantification of cell viability) and high resolution electron microscopy imaging (qualitative analysis of the microbial cell morphology and internal structure) could be used together to elucidate conceivable mechanisms of action.

2. Materials and Methods

2.1. Materials

2.1.1. Reagents. Milli-Q water has been used throughout. Magnesium methoxide, 7−8% in methanol, was obtained from Alfa-Aesar; absolute ethanol was purchased from Panreac. 3-(4,5-Dimethylthiazol-2-yl)-2,5-diphenyltetrazolium bromide (MTT) was purchased from Invitrogen. Resazurin sodium salt and TBX agar from Sigma-Aldrich.

2.1.2. Eukaryotic cells. Vero cells (monkey kidney epithelial cells) were purchased from the American Type Culture Collection (ATCC, Manassas, VA, USA, number CCL-81). Dulbecco's modified Eagle's medium (DMEM), Phosphate-Buffered Saline (PBS), Dulbecco's Phosphate-Buffered Saline (DPBS) were purchased from Lonza.

2.1.3. Microorganisms. *Escherichia coli* DH5-alpha as Gram-negative (G-) bacteria and *Bacillus subtilis* 1904-E as Gram-positive (G+) bacteria were used in the assays. Luria-Bertani (LB) liquid medium (Miller's formulation) and Nutrient Broth (NB) liquid medium were freshly prepared and sterilized by autoclave. Trypticase Soy Agar plates were purchased from Thermo Scientific ™.

2.1.4. Test papers. Three different paper samples from the last third of the 18th century were used in this study. The papers differ in colour, thickness and roughness.

2.2. Methods summary

2.2.1. Bacterial growth curves. Bacterial growth was recorded measuring the optical density (OD) of the samples at 600 nm every one hour (0-8 hours) using a microplate reader (Thermo Scientific MULTISKAN GO). Results were compared with the OD variation of a control culture containing only bacteria. All controls and antibacterial assays were replicated in sextuplet to verify the reproducibility of the results and to calculate the mean values and standard deviations.

2.2.2. Cell viability assays. Cell viability was measured using a Thermo Scientific Multiskan GO plate reader. Each measurement was repeated five times to obtain the mean values and standard deviations.

2.2.3. Environmental Scanning Transmission Electron Microscopy (ESTEM): Data were collected on a Quanta FE6-250 (FEI Company) field emission SEM for high-resolution imaging working at low vacuum mode using a STEM detector.

2.2.4. Powder X-Ray Diffraction (PXRD). The crystalline phase of the nanoparticles was verified using PXRD spectra obtained using a D-Max Rigaku instrument equipped with a rotating Cu anode and a graphite monocromator (therefore working with $K_{\alpha 1}$=1.5405 Å). The diffractometer worked at 40 kV and 80 mA. Data were recorded in the 2θ range between 10° and 90° by using a step of 0.03° and 1 s/step.

2.2.5. Scanning Electron Microscopy (SEM): SEM images and energy dispersive X-ray spectroscopy (EDX) spectra were acquired using a field emission SEM Inspect F50 with an EDX system INCA PentaFETx3 (FEI Company, Eindhoven, The Netherlands) in the energy range 0-30 keV.

2.2.6. Transmission Electron Microscopy (TEM). Preliminary observation of the synthesized particles was carried out by Bright Field (BF) imaging in a FEI Tecnai T20 microscope operating at 200 kV. The samples were prepared by resuspending the powder in ethanol under sonication, putting a drop of the suspension directly on a TEM carbon grid, and letting it dry in air atmosphere. From different TEM images, an estimation of the diameter distribution has been obtained using Digital Micrograph® (Gatan Inc., Pleasanton, TX, USA) and OriginLab® (OriginLab, Northampton, MA, USA) software to measure the diameters of more than 100 NPs and for the frequency count statistical analysis respectively. Observation of microbial cells after incubation with nanoparticles was carried out using the same machine operating at 80 kV. The biological samples were prepared by fixation with glutaraldeyhde, embedding in resin and cutting with a microtome.

2.3 Nanoparticle synthesis

MgO nanoparticles were synthesized by sol-gel method through a modification of protocols already reported in literature (Bokhimi et al., 1996). Briefly, 3.6 mL of magnesium methoxide, $Mg(OCH_3)_2$, (2.4 mmol) were added to 20 mL of absolute ethanol under ultrasonication and subsequently 0.9 mL of water (50 mmol) were added to the mixture. The sol was left in the ultrasonic bath for 30 min. The mixture was then kept under gentle stirring for 36 h to facilitate gelification.

The water/ethanol gel suspension was stirred in an oil bath and underwent a progressive increase of the temperature from 70 to 90 °C over a period of 5 h, before being completely dried in air until a fine magnesium dihydroxide powder was obtained. The final step involved annealing this powder at 600 °C for 30 min to obtain the complete oxidation of $Mg(OH)_2$ to MgO. Yield = 87 mg (dry particles).

2.4 Eukaryotic cell viability assay in presence of MgO nanoparticles

Vero cells were cultured in Dulbecco's modified Eagle's medium (DMEM), supplemented with 10% foetal bovine serum (FBS), 5% glutamine and 5% penicillin/streptomycin. Cell cultures were maintained at 37 °C and equilibrated in 5% CO_2 and air. Cell viability and proliferation in the presence of MgO NPs were analysed by 3-(4,5-dimethylthiazol-2-yl)-2,5-diphenyl tetrazolium bromide (MTT) assay (Carmichael, et al., 1987; Mai et al., 2012). For the cytotoxicity assay $5x10^3$ cells were seeded a 96-well plate and grown for 24 h, then the medium was replaced with fresh medium containing the MgO NPs at various concentrations. At the end of the 24 h incubation period, the medium was replaced with fresh medium and 20 µL of MTT dye solution (5 mg/mL in PBS) was added to each well. After 3 h of incubation at 37 °C and

176 5% CO_2, the medium was removed and formazan crystals were dissolved in 100 µL of DMSO. The absorbance of each well was read on a microplate reader at 570 nm. The relative cell
178 viability (%) related to control wells containing cells incubated without nanoparticles was calculated by $ABS_{test}/ABS_{control}$ x 100. Each measurement was repeated five times to obtain the
180 mean values and the standard deviation.

182 **2.5 Bacterial cell proliferation assays in presence of MgO nanoparticles**

The experiments were performed with two bacterial strains, *Escherichia coli* DH5-alpha and
184 (Gram -) *Bacillus subtilis* 1904-E (Gram +). The bacteria was pre-inoculated in culture medium (Luria-Bertani (LB) medium for *E. coli* and Nutrient Broth (NB) for *B. subtilis)* and kept under
186 shaking (180 rpm) at 37 °C for 15 hours. A dilution from this culture was used for the following tests, corresponding to an inoculum of $1x10^7$ CFU/mL. Firstly, culture medium was
188 supplemented with the required amounts of MgO NPs in order to obtain the desired concentration in the sample suspension. MgO NPs were therefore dispersed previously in the
190 corresponding medium for 30 minutes under ultrasonication. Thereafter bacterial inoculum was added to the MgO NP/culture medium dilutions and the bacterial growth curves were recorded
192 over a period of 24 h by measuring the optical density (OD) of the samples at 600 nm. Results were compared with the OD variation of a control culture containing *E. coli* or *B. subtilis*
194 without any NPs. To verify the data, the colony-forming ability (cell viability) of *E. coli* or *B. subtilis* incubated with different concentrations of MgO NPs was tested by plating properly
196 diluted aliquots of the samples in the logarithmic phase (4 h incubation) on nutrient agar plates and incubating the plates at 37 °C overnight.

198 **2.6 Resazurin cell viability assays**

Cell viability was analysed using a Resazurin (7-Hydroxy-3H-phenoxazin-3-one 10-oxide)
200 assay in a 96-well plate. A bacterial inoculum ($1x10^7$ CFU/mL) of *E. coli* (in LB media) and *B. subtilis* (in NB media) was supplemented with different concentrations of MgO NPs as in the
202 growth inhibition assay and a blank sample (bacteria without MgO NPs) was also included in the assay as negative control. Once the microbial cultures had been grown for a total of 24 h,
204 30 µL of 0.1 mg/mL Resazurin (in LB or NB medium) was added to each well and incubated in the dark at 37 °C for 1 h under stirring.

206 **2.7 LIVE/DEAD® assay**

Cell viability was analysed also by a LIVE/DEAD® fluorescence assay. A bacterial inoculum
208 ($1x10^7$ CFU/mL) of *E. coli* (in LB media) and *B. subtilis* (in NB media), was supplemented with MgO NPs at a final concentration of 1.5 mg/ml. A sample without MgO NPs was also
210 included in the assay as negative control. After 24 hours of incubation at 37 ºC with stirring, the solutions were stained with the LIVE/DEAD® BacLight™ Bacterial Viability Kit in a
212 1:500 dilution and incubated for 15 minutes in the dark. Then 10 µL of the stained samples were extended over a slide and the bacteria were visualized with a Nikon ECLIPSE Ti
214 epifluorescence microscope. The experiments were performed with three different samples of paper (differing in their colour, thickness and roughness) from the 18th century from the
216 Archives of Real Jardín Botánico-CSIC (Madrid, Spain).

2.8 Agar diffusion test

218 A modified Kirby-Bauer disk diffusion technique was used. In order to test the particle release capacity of the paper samples, each of the three papers were cut in 6 mm discs and they were
220 impregnated with a 15 mg/mL MgO NPs solution. Another disc of each paper was impregnated with a 100 µg/mL Ampicillin solution as a positive control. To test the diffusion ability of the

MgO NPs, also a Whatman® Antibiotic Assay Discs (6 mm) was impregnated with the 15 mg/mL MgO NPs solution and another one with the 100 µg/mL Ampicillin solution. All these papers, together with a non-impregnated Whatman® Disc as negative control, were placed in an agar plate previously inoculated with an *E. coli* lawn. After 24 h of incubation at 37 ºC, the inhibition halo around the samples was measured.

2.9 Inductively Coupled Plasma Atomic Emission Spectroscopy (ICP-AES) analysis of nanoparticle interaction with microbial cells

E. coli and *B. subtilis* samples of $1x10^7$ CFU/mL in LB or NB medium, respectively were incubated with 1.5 mg/mL of NPs overnight. Bacterial cells were then separated from the supernatant by centrifugation. Both pellet and supernatant were digested with a 3:1 HCl/HNO_3 mixture and the Mg concentration was evaluated by ICP-AES analysis. Each sample was measured in triplicate to obtain mean values.

2.10 Antimicrobial assays on paper samples

18^{th} century paper samples were obtained from the leftovers of the Herbarium sheets conserved in the Archives of the Real Jardín Botánico (Madrid, Spain). Paper numbers 1 and 3 were used to keep dried plants, whereas paper number 2 was the usual text document accompanying the plant samples. These paper samples were cut in 4x4 cm squares and each paper was placed in a sterile Petri dish. Each paper was impregnated with 500 µL of a 10 mg/mL MgO NPs solution in small drops using a micropipette, before being sterilized under UV for 15 min and allowed to dry in a sterile environment. This process was performed twice on each paper to ensure a homogenous coating of MgO NPs. Once the papers were dry, an *E. coli* solution (10^4 CFU/mL) was sprayed, twice, over the paper samples with MgO NPs and over the negative control samples (papers without MgO NPs). To detect the bacterial growth over the paper samples TBX agar was used, which contains X-β-D-glucuronide, a chromogenic compound hydrolyzed by the β-glucuronidase, an *E. coli* enzyme, which makes the *E. coli* colonies turn green-blue on an agar plate. A first layer of TBX agar was added over all the paper samples covering all the surface of the paper. When the medium solidified, a second layer was added. The papers were then incubated for 48 h at 37 ºC whereupon the bacterial colonies were clearly observable with the naked eye.

2.11 Environmental Scanning Electron Microscopy (ESEM) analyses

ESEM was used to analyse both bacterial cell morphology, after incubation with the MgO NPs, and the appearance of paper samples, after covering with MgO NPs. All samples were analysed in a Quanta FE6-250 (FEI Company) field emission ESEM for high-resolution imaging working at low vacuum mode. Bacterial cell samples were prepared in the same way as in the fluorescence assay, including also a negative control of bacteria culture without MgO NPs, and after the 24 h of incubation they were fixed using the following procedure: They were centrifuged 10 min at 1,400 rpm (300 G), the supernatant was removed and the pellet was resuspended into 1.5 mL of sterile PBS. This procedure was repeated twice and the pellet was finally resuspended into 1.5 mL phosphate buffer 10 mM pH 7.2 + 2.5% glutaraldehyde. Bacteria were incubated with this solution for two hours in a wheel at room temperature and they were washed twice with 1.5 mL of PBS. Finally they were resuspended in water. The sample was analysed without any previous treatment directly from water suspension.

3. Results and Discussion

A sol-gel method was chosen for the synthesis of the MgO NPs since it is represents a simple, cheap, reproducible an scalable synthetic process, which also allows for a reasonable control of the size of the nanoparticles and their subsequent properties. The synthetic conditions were

optimized in terms of reactant amounts, pH conditions, reaction time and temperature to obtain the desired product, as reported in the Experimental Section. After the condensation step of the sol-gel process and the first drying step, $Mg(OH)_2$ NPs were obtained and a proper annealing process was necessary to convert this product into crystalline MgO NPs. X-Ray Diffraction (XRD) analysis was performed before and after the annealing to determine the final crystalline structure of the material. The complete transformation into MgO crystalline phase was confirmed, excluding any presence of $Mg(OH)_2$ phase, and demonstrating that an annealing temperature of 600 °C, maintained during 30 minutes, was necessary to obtain the cubic MgO structure observed in the XRD spectrum. XRD spectrum of MgO NPs is reported in Figure S1 in the Supplementary Information. From this spectrum it is also possible to estimate the average size of the crystallites by means of the Scherrer formula $d = k\lambda/\beta\cos(\theta)$, where λ is the Cu−$K_{\alpha 1}$ X-ray wavelength, β is the full width at half-maximum, and k is the shape factor. The calculated average size for the synthesized NPs was 10 nm.

The size and shape of the MgO NPs were analyzed by BF-TEM (Figure 1). Figure 1A is a BF-TEM image of the nanoparticles deposited on a carbon film TEM grid after solvent evaporation, while Figure 1B is a magnification of the previous one, reported for sake of comprehension. Figure 1C shows an estimation of the NP size obtained from a statistical frequency count of the particle diameters measured from TEM images. As observed from the figure, particle sizes range from 8 to 20 nm, with 9-15 nm being the most prevalent population. This estimation is coherent with the size calculated from the XRD spectrum through Scherrer equation. From the TEM image, it can also be observed that NPs tend to form small aggregates of about 5-10 NPs with an aggregate size of about 100 nm but it could not be excluded that this effect could be produced during the sample preparation as a drying artifact (Domingos et al., 2009).

The antibacterial effect of the MgO NPs was verified using two methods: by studying how their presence affected bacterial growth (cell proliferation assays) and determining the minimum inhibitory concentration (MIC) of the particles using a colorimetric resazurin cell viability assay (Figure S2). These studies investigated the antimicrobial effect of MgO NPs at different concentrations against the Gram-negative bacteria *Escherichia coli* (*E. coli*) and the Gram-positive *Bacillus subtilis* (*B. subtilis*) using dispersions of MgO NPs in Luria-Bertani (LB) or Nutrient Broth (NB) growth medium, respectively. The study of growth curves of bacterial cells in suspension measures the turbidity of the culture suspension as optical density (OD) of the medium and allows the determination of the rate of bacterial growth over the 24 h incubation period (Figure 2). The dispersed MgO NPs showed high antiproliferative activity against both strains of bacteria. Full inhibition of bacterial growth was observed at concentrations of 1.50 mg/mL and 0.75 mg/mL for *E. coli* and *B. subtilis* respectively. The results obtained from optical density analyses were commensurate with the MIC values from the spectrophotometric resazurin cell viability assays, which clearly show that MgO NPs are bactericidal and how Gram+ *B. subtilis* was more susceptible to the MgO NPs than Gram- *E. coli*.

Importantly, we have also demonstrated that the particles did not produce cytotoxic effects in a kidney epithelial cell line (Vero cells line) over the same concentration range (Figure S3). This evidence is commensurate with the aforementioned literature, which indicates that MgO NPs are not cytotoxic to mammalian cell lines and are safe to use, at least to the highest tested concentration of 1 mg/mL.

In order to complement these results, both *E. coli* and *B. subtilis* were incubated with the MgO NPs and stained with a LIVE/DEAD® BacLight™ Bacterial Viability Kit to determine the viability of the bacteria after the incubation. The samples incubated with the particles present lower bacterial density than the bacterial culture without the MgO NPs due to the antiproliferative effect of the MgO (Figure S4).

316 Although the antibacterial assays already stated the potent antibacterial activity of the MgO NPs, Electron Microscopy observations were performed to obtain in-depth information about 318 the effect of the NPs on bacterial cells. Environmental Scanning Transmission Electron Microscopy (ESTEM) imaging of bacteria incubated with the MgO NPs can provide additional 320 visible insight into bacteria morphology and health. ESTEM demonstrated how the MgO NPs clearly elicited distinct responses from the bacterium cells, indicative of different particle–322 bacterium interactions (Figure 3). Both bacterial strains incubated with MgO NPs showed evidence of stress and damage including general loss of cell shape, cell membrane damage and 324 leakage of cytoplasmic material. *B. subtilis* appeared to show signs of sporulation, an indicator of cell stress.

326 Initial Electron Paramagnetic Resonance spectroscopy (data not shown) showed that reactive oxygen species (ROS) were not produced under the *in vitro* conditions reported herewithin. 328 Thus, to begin to understand the mechanism of action, Transmission Electron Microscopy (TEM) was used to determine the interaction of the MgO NPs with *E. coli* in particular (Figure 330 4). Bacteria were incubated with different concentrations of MgO NPs for a 24 h period whereupon the cells were post-fixed, dehydrated, embedded in epoxy resin and sliced into 10 332 μm slivers using a microtome. Our initial aim was to attempt to identify the location of MgO NPs (or aggregates thereof) internalised within the bacteria or associated with the cell surface. 334 Unfortunately, and as may be expected, the low electron density of magnesium atoms meant that this particular element could not be distinguished from the vast amount of carbon in the 336 bacterial cells. In Figure 4 images of cells treated with 0.5 and 1 mg/mL of MgO NPs are reported (c and d) together with a control of untreated cells (a) and a control of cells grown in 338 a medium at pH 9. This control is necessary due to the increase of the pH of the medium induced by the presence of MgO NPs. TEM imaging of MgO NP-treated bacteria emphasised the 340 general damage of the bacterial envelope, as previously observed with ESEM. Some damage could be addressed to the increase of the pH of the medium, for example condensation of the 342 cytoplasmic material that can be observed in Figure 4b and c and that is in agreement with the literature. Although the increase in the pH value was responsible for some damages to the 344 bacterial cells, it is clear from Figure 4d that at higher NP concentrations the effect of NPs caused a permeabilisation of the bacterial envelope and leakage of the cytoplasmic material. A 346 concentration of 1 mg/mL NPs has been used in this experiment (below the MIC of 1.5 mg/mL) because this represents the highest NP concentration at which the observation of bacterial cells 348 was still possible, since at higher concentrations their growth was completely inhibited.

The significant interaction of MgO NPs with bacterial cells was demonstrated by elemental 350 analysis of bacteria incubated with MgO NPs, with *E. coli* displaying the most prominent magnesium content, retaining as much as 25% of the MgO NPs added to the medium (Table 352 1). Based on these results, it remains to be determined whether the MgO NPs interact with the cell membrane or actually internalise inside the bacteria, although this void currently forms part 354 of our ongoing research efforts.

A variety of 18th century paper samples were obtained from the Archives of the Real Jardín 356 Botánico (Madrid) in order to test the applicability of the MgO NPs in real samples (Figure S5). Three paper samples covering a variety of coarseness and porosity were selected from those 358 provided. Establishing an efficient means of evaluating the activity of the particles *in situ* was one of the key priorities of this research and various different methods of evaluating and 360 quantifying the microbial growth on the paper surfaces were investigated. In the first instance, the papers were cut into circles to perform a modified Kirby-Bauer disk diffusion technique. 362 All the papers, including two circles of Whatman® Antibiotic Assay Discs were impregnated with an MgO NP suspension (disc 1) and with an Ampicillin solution (disc 2) as a control. After 364 the incubation over an *E. coli* lawn, the only sample which generated an inhibition halo was the

Whatman® disc impregnated in Ampicillin. Thus, it can be deduced that the MgO NPs do not diffuse on the agar meaning that there was no release of the MgO NPs from the Real Jardín Botánico papers into the agar medium (Figure S6). We established a TBX agar method as a convenient means of detecting and quantifying the growth of *E.coli* on the paper samples. TBX Agar contains X-β-D-glucuronide, a chromogenic compound hydrolyzed by the β-glucuronidase (an *E. coli* enzyme) making the *E. coli* colonies turn green-blue on a conventional agar plate. The papers were therefore cut into 4x4 cm squares and placed in a sterile Petri dish and was impregnated with a 10 mg/mL MgO NPs solution and allowed to dry (see Materials & Methods). Once dry the papers were sprayed twice with a 10^4 CFU/mL *E. coli* suspension. In our methodology the papers were each covered by a fine layer of TBX agar and when the medium solidified the process was repeated to obtain a complete homogeneous covering. The papers were then incubated for 48 h at 37 ºC. Afterwards the treated and untreated papers were compared and counting of the green-blue *E. coli* colonies clearly illustrated the efficacy of the MgO NPs for preventing colonisation of the paper samples (Figure 5). In addition, ESTEM images of 18th century papers 1-3 treated with MgO NPs confirmed that the MgO NPs provide a homogeneous dispersion over the surface of the papers, where particles were clearly visible penetrating the pores and fibres of the paper to provide a deep protective coating layer (see Figure S7).

4. Conclusions

The powerful antibacterial activity of nano-magnesium oxide particles was used to protect various 18th century papers from bacterial colonisation. The combination of antibacterial assays and high resolution electron microscopy imaging has shown how the particles cause oxidative stress, cell membrane leakage and cell death and furthermore, this methodology has verified that the paper surfaces were covered by a homogenous nanoparticle coating which does not alter the aesthetics of the paper. Our on-going research efforts are currently centred on evaluating and understanding the activity of these nanoparticles against different strains of bacteria and fungi that are common to museums, archives and library collections.

5. Acknowledgements

Financial support by the Fundación General CSIC (S.G.M., Programa ComFuturo), Fondo Social Europeo-Gobierno de Aragón (J.M.F, L.D.M., I.F.C. & S.G.M.) is gratefully acknowledged. Access to and use of the Advanced Microscopy Laboratory (University of Zaragoza) and to the XRD facility of the Servicio General de Apoyo a la Investigación of the Universidad de Zaragoza is gratefully acknowledged. The authors also thank Mario Soriano (Centro de Investigación Principe Felipe, Valencia, Spain), Rodrigo Fernández-Pacheco and Carlos Cuestas (Laboratorios de Microscopia Avanzada de la Universidad de Zaragoza) for their valuable technical support in electron microscopy experiments.

6. References

Asghar Ariafar, A., Afsharpour, M., Samanian, K. 2017. Use of TiO_2/chitosan nanoparticles for enhancing the preservative effects of carboxymethyl cellulose in paper-art-works against biodeterioration. International Biodeterioration & Biodegradation, in-press (corrected proof). https://doi.org/10.1016/j.ibiod.2017.04.025.

Baglioni, M., Giorgi, R., Berti, D., Baglioni, P. 2012. Smart cleaning of cultural heritage: a new challenge for soft nanoscience, Nanoscale 4, 42-53. doi: 10.1039/C1NR10911A.

Baglioni, P., Carretti, E., Chelazzi, D. 2015. Nanomaterials in art conservation. Nature Nano. 10, 287-290. doi:10.1038/nnano.2015.38.

410 Bokhimi, X., Morales, A., Lopez, T., Gomez, R. J. 1995. Crystalline Structure of MgO Prepared by the Sol-Gel Technique with Different Hydrolysis Catalysts. Solid State Chem. 115, 412 411−415. https://doi.org/10.1006/jssc.1995.1152.

Bondarenko, O., Juganson, K., Ivask, A. et al. 2013. Toxicity of Ag, CuO and ZnO 414 nanoparticles to selected environmentally relevant test organisms and mammalian cells in vitro: a critical review. Arch. Toxicol. 87, 1181. https://doi.org/10.1007/s00204-013-1079-4.

416 Carmichael, J., Degraff, W. G., Gazdar, A. F., Minna, J. D., Mitchell, J. B. 1987. Evaluation of a tetrazolium-based semiautomated colorimetric assay: assessment of radiosensitivity. Cancer 418 Res. 47, 936-946.

Dizaj, S.M., Lotfipour, F., Barzegar-Jalali, M., Zarrintan, M.H., Adibkia, K. 2014. 420 Antimicrobial activity of the metals and metal oxide nanoparticles. Mater. Sci. Eng. C: Mater. Biol. Appl. 44, 278-284. https://doi.org/10.1016/j.msec.2014.08.031.

422 Domingos, R.F., Baalouscha, M.A., Ju-Nam, Y., Reid, M.M., Tufenkji, N., Lead, J.R., Leppard, G.G., Wilkinson, K.J. 2009. Characterizing Manufactured Nanoparticles in the Environment: 424 Multimethod Determination of Particle Sizes. Environ. Sci. Technol. 43, 7277-7284. DOI: 10.1021/es900249m.

426 Ge, S., Wang, G., Shen, Y., Zhang, Q., Jia, D., Wang, H. 2011. Cytotoxic effects of MgO nanoparticles on human umbilical vein endothelial cells in vitro. IET Nanobiotechnology 5, 36-428 40. http://ieeexplore.ieee.org/document/5754012/.

Ghobadian, M., Nabiuni, M., Parivar, K., Fathi, M., Pazooki, J. 2015. Toxic effects of 430 magnesium oxide nanoparticles on early developmental and larval stages of zebrafish (Danio rerio). Ecotoxicol. Environ. Saf. 122, 260-267. https://doi.org/10.1016/j.ecoenv.2015.08.009.

432 Gutarowska, B., Skora, J., Zduniak, K., Rembisz, D. 2012. Analysis of the sensitivity of microorganisms contaminating museums and archives to silver nanoparticles. International 434 Biodeterioration & Biodegradation 68, 7-17. https://doi.org/10.1016/j.ibiod.2011.12.002.

Hajipour, M.J., Fromm, K.M., Ashkarran, A.A., Jiménez de Aberasturi, D., de Larramendi, 436 I.R., Rojo, T., 2012. Antibacterial properties of nanoparticles. Trends Biotechnol. 30, 499–511. https://doi.org/10.1016/j.tibtech.2012.06.004.

438 He, Y., Ingudam, S., Reed, S., Gehring, A., Strobaugh Jr., T. P., Irwin, P. 2016. Study on the mechanism of antibacterial action of magnesium oxide nanoparticles against foodborne 440 pathogens. J. Nanobiotechnology 14, 54. https://doi.org/10.1186/s12951-016-0202-0.

Koizhaiganova, M., Yaşa, I., Gülümser, G. 2015. Assessment of antibacterial activity of lining 442 leather treated with silver doped hydroxyapatite, International Biodeterioration & Biodegradation 105, 262-267. https://doi.org/10.1016/j.ibiod.2015.09.017.

444 Krishnamoorthy, K., Moon, J. Y., Hyun, H. B., Cho, S. K. Kim, S.-J. 2012. Mechanistic investigation on the toxicity of MgO nanoparticles toward cancer cells, J. Mater. Chem. 22, 446 24610–24617. doi: 10.1039/C2JM35087D.

La Russa, M. F., Ruffolo, S. A., Rovella, N., Belfiore, C. M., Palermo, A. M., Guzzi, M.T., 448 Crisci, G. M. 2012. Multifunctional TiO_2 coatings for Cultural Heritage. Prog. Org. Coat. 74, 186-191. https://doi.org/10.1016/j.porgcoat.2011.12.008.

450 La Russa, M.F., Macchia, A., Ruffolo, S.A., De Leo, F., Barberio, M., Barone, P., Crisci, G.M., Urzì, C. 2014. Testing the antibacterial activity of doped TiO_2 for preventing biodeterioration

452 of cultural heritage building materials. International Biodeterioration & Biodegradation 96, 87-
96. http://dx.doi.org/10.1016/j.ibiod.2014.10.002

454 La Russa M.F., Rovella, N., Alvarez de Buergo, M., Belfiore, C. M., Pezzino, A., Crisci, G.
M., Ruffolo, S. A., 2016. Nano-TiO_2 coatings for cultural heritage protection: The role of the
456 binder on hydrophobic and self-cleaning efficacy. Prog. Org. Coat. 91, 1-8.
https://doi.org/10.1016/j.porgcoat.2015.11.011.

458 Leung, Y.H., Ng, A.M., Xu, X., Shen, Z., Gethings, L.A., Wong, M.T. 2014. Mechanisms of
antibacterial activity of MgO: non-ROS mediated toxicity of MgO nanoparticles
460 towards *Escherichia coli*. Small 10, 1171–1183. http://doi.org/10.1002/smll.201302434.

Li, W.-R., Sun, T.-L., Zhou, S.-L., Ma, Y.-K., Shi, Q.-S., Xie, X.-B., Huang, X.-M. 2017. A
462 comparative analysis of antibacterial activity, dynamics, and effects of silver ions and silver
nanoparticles against four bacterial strains. International Biodeterioration & Biodegradation
464 123, 304-310. https://doi.org/10.1016/j.ibiod.2017.07.015.

Mai, T.-T., Moon, J.-Y., Song, Y.-W., Viet, P.-Q., Phuc, P.-V., Lee, J.-M., Yi, T.-H., Cho, M.,
466 Cho, S.-K. 2012. Ginsenoside F2 induces apoptosis accompanied by protective autophagy in
breast cancer stem cells. Cancer Lett. 321, 144-153. doi: 10.1016/j.canlet.2012.01.045.

468 Park, J. Y., Lee, Y.-J., Jun, K.-W., Baeg, J.-O., Yim, D. J. 2006. Chemical synthesis and
characterization of highly oil dispersed MgO nanoparticles, J. Ind. Eng. Chem. 12, 882–887.
470 https://www.cheric.org/PDF/JIEC/IE12/IE12-6-0882.pdf.

Pietrzak, K., Puchalski, M., Otlewska, A., Wrzosek, H., Guiamet, P., Piotrowska, M.,
472 Gutarowska, B. 2017. Microbial diversity of pre-Columbian archaeological textiles and the
effect of silver nanoparticles misting disinfection, Journal of Cultural Heritage 23, 138-147.
474 https://doi.org/10.1016/j.culher.2016.07.007.

Portillo, R., Lopez, T., Gomez, R., Bokhimi, X., Morales, A., Novaro, O. 1996. Magnesia
476 Synthesis via Sol−Gel: Structure and Reactivity. Langmuir 12, 40−44. DOI:
10.1021/la940694n.

478 Raghupathi, K. R., Koodali, R. T., Manna, A. C. 2011. Size-Dependent Bacterial Growth
Inhibition and Mechanism of Antibacterial Activity of Zinc Oxide Nanoparticles. Langmuir 27
480 (7), 4020–4028. http://pubs.acs.org/doi/abs/10.1021/la104825u.

Reddy, K. M., Feris, K., Bell, J., Wingett, D. G., Hanley, C., Punnoose, A. 2007. Selective
482 toxicity of zinc oxide nanoparticles to prokaryotic and eukaryotic systems. Appl Phys Lett. 90,
2139021–2139023. https://doi.org/10.1063/1.2742324.

484 Ruffolo S. A., La Russa, M. F., Malagodi, M., Oliviero Rossi, C., Palermo, A. M., Crisci, G.
M. 2010. ZnO and $ZnTiO_3$ nanopowders for antimicrobial stone coating. App. Phys. A. 100,
486 829-834. https://doi.org/10.1007/s00339-010-5658-4.

Shirakawa, M. A., John, V. M., Mocelin, A., Zilles, R., Toma, S.H., Araki, K., Toma, H.E.,
488 Thomaz, A. C., Gaylarde, C. C. 2016. Effect of silver nanoparticle and TiO_2 coatings on biofilm
formation on four types of modern glass. International Biodeterioration & Biodegradation 108,
490 175-180. https://doi.org/10.1016/j.ibiod.2015.12.025.

Sierra-Fernandez, A., Gomez-Villalba, L.S., Rabanal, M.E., Fort, R. 2017. New nanomaterials
492 for applications in conservation and restoration of stony materials: A review, Materiales de
Construcción 67, e107. http://dx.doi.org/10.3989/mc.2017.07616.

494 Sierra-Fernandez, A., De la Rosa-García, S. C., Gomez-Villalba, L. S., Gómez-Cornelio, S., Rabanal, M. E., Fort, R., Quintana, P. 2017. Synthesis, Photocatalytic, and Antifungal
496 Properties of MgO, ZnO and Zn/Mg Oxide Nanoparticles for the Protection of Calcareous Stone Heritage. ACS Appl. Mater. Interfaces 9, 24873–24886.
498 http://pubs.acs.org/doi/abs/10.1021/acsami.7b06130.

Skóra, J., Gutarowska, B., Pielech-Przybylska, K., Stępień, L., Pietrzak, K., Piotrowska, M.
500 Pietrowski, P. 2015. Assessment of microbiological contamination in the work environments of museums, archives and libraries. Aerobiologia 31, 389-401. https://doi.org/10.1007/s10453-
502 015-9372-8.

Sterflinger, K., Pinzari, F. 2012. The revenge of time: fungal deterioration of cultural heritage
504 with particular reference to books, paper and parchment, Environmental Microbiology 14, 559–566. doi: 10.1111/j.1462-2920.2011.02584.x.

506 Sterflinger, K., Piñar, G., 2013. Microbial deterioration of cultural heritage and worksvof art - tilting at windmills? Appl. Microbiol. Biotechnol. 97, 9637-9646.

508 Srinivasan, V., Bhavan, P.S., Rajkumar, G., Satgurunathan, T., Muralisankar, T., 2017. Dietary Supplementation of Magnesium Oxide (MgO) Nanoparticles for Better Survival and Growth
510 of the Freshwater Prawn Macrobrachium rosenbergii Post-larvae. Biol Trace Elem Res. 177(1), 196-208. doi: 10.1007/s12011-016-0855-4.

512 Tang, Z.-X., Fang, X.-J., Zhang, Z.-L., Zhou, T., Zhang, X.-Y., Shi, L.-E., 2012. Nanosize MgO as antibacterial agent: preparation and characteristics, Braz. J. Chem. Eng. 29, 775–781.
514 http://dx.doi.org/10.1590/S0104-66322012000400009.

Tang Z.-X., Lv B.F. 2014. MgO nanoparticles as antibacterial agent: preparation and activity.
516 Braz. J. Chem. Eng. 31, 591–601. doi: 10.1590/0104-6632.20140313s00002813.

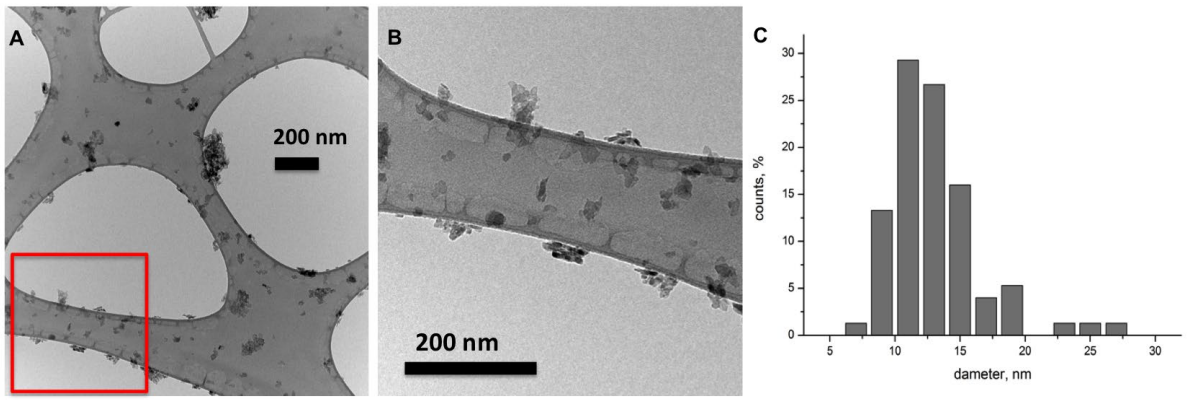

518 **Figure 1.** BF-TEM images of MgO NPs (B is a magnification of the area selected in A) and estimated size dispersion histogram (C).

520

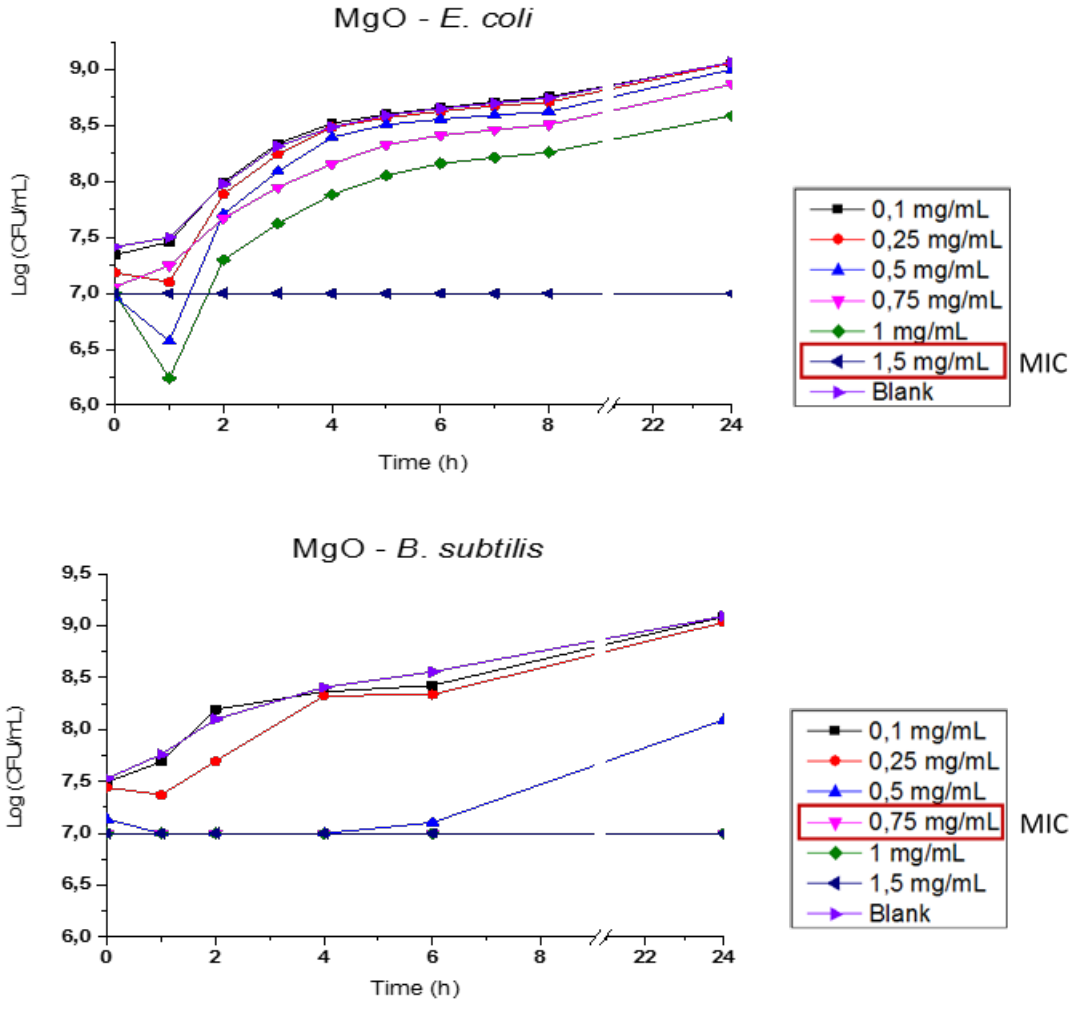

522

524 **Figure 2.** *E. coli* and *B. subtilis* growth curves starting from a concentration of 10^7 CFU/mL in LB (or NB) medium at different MgO NP concentrations. MIC for *E. coli* is 1.5 mg/mL while MIC for *B. subtilis* is lower, 0.75 mg/mL. The blank control references in both graphs refer to *E. coli* or *B. subtilis* 526 (starting from a concentration of 10^7 CFU/mL) in culture medium. Antibacterial assays were repeated on several occasions and replicated a total of six times to calculate mean values and associated standard 528 deviations.

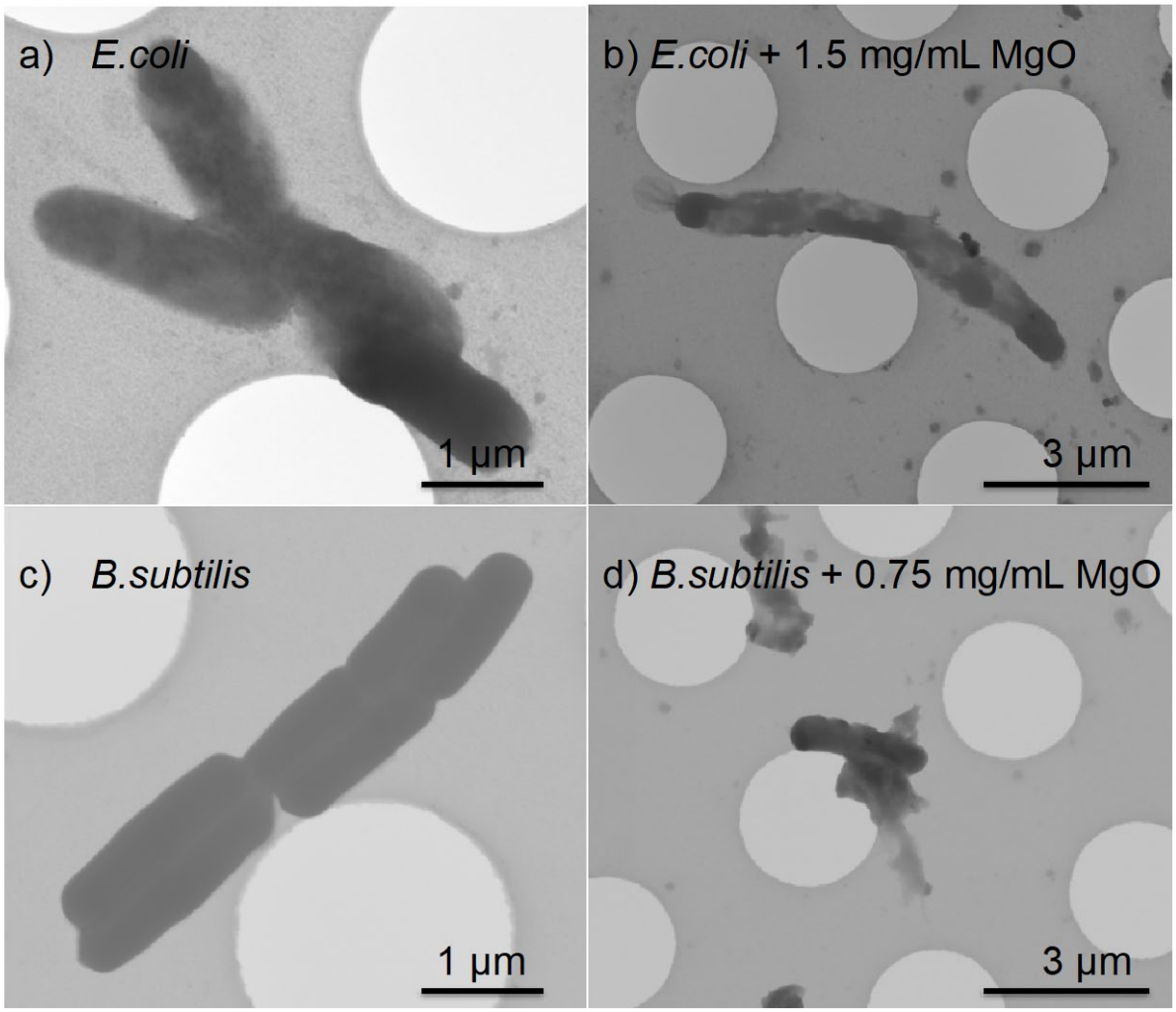

530 **Figure 3.** Environmental STEM images of *E. coli* and *B. subtilis* incubated with MgO NPs at the corresponding MICs, where a) *E. coli* control cells; b) *E. coli* incubated with 1.5 mg/mL MgO NPs; c)
532 *B. subtilis* control cells and d) *B. subtilis* incubated with 0.75 mg/mL MgO NPs.

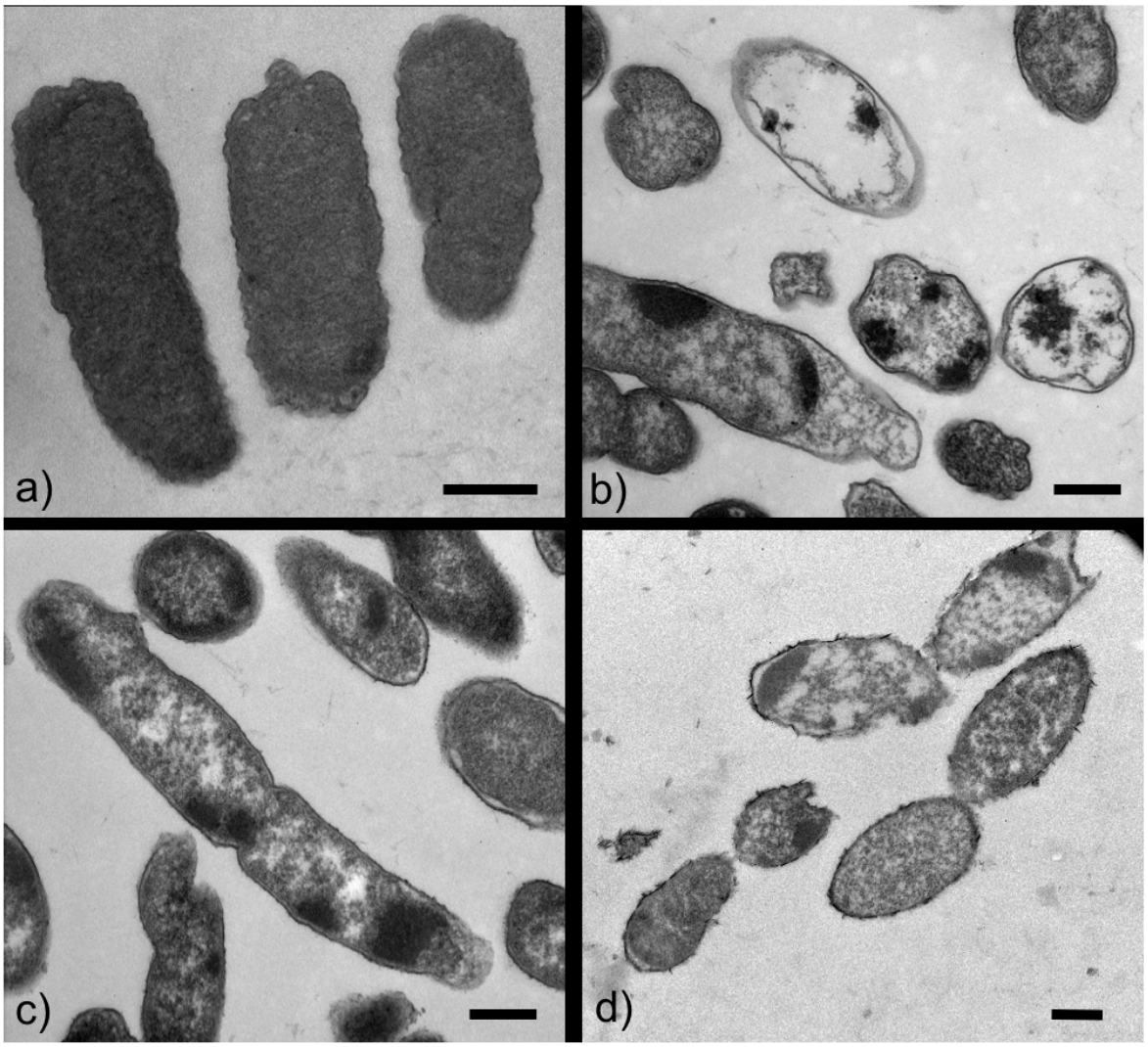

Figure 4. Transmission Electron Microscopy (TEM) images of *E. coli* culture submitted to different treatments*:* control cells without any treatment (a); cells growth in the medium at pH 9 (b); cells incubated with 0.5 mg/mL MgO NPs (c) and cells incubated with 1 mg/mL MgO NPs (d). The predominant effect exerted on the bacterium cells by the MgO NPs is the loss of normal healthy shape and condensation of the cytoplasmic material (c); however, leakage of the cytoplasmic material also occurs (d). Scale bars correspond to 500 nm.

Table 1. ICP-AES elemental quantification of the Mg content of *E. coli* and *B. subtilis* cells incubated with MgO NPs along with negative control samples (bacteria without MgO NPs).

Sample	**Mg (mg/L)**	**% Mg w.r.t inoculation**
MgO NPs	13.5	100
E. coli + MgO NPs	3.3	24.7
B. subtilis + MgO NPs	<0.2	2.4
E. coli (control)	<0.02	<0.2
B. subtilis (control)	0.02	0.2

544

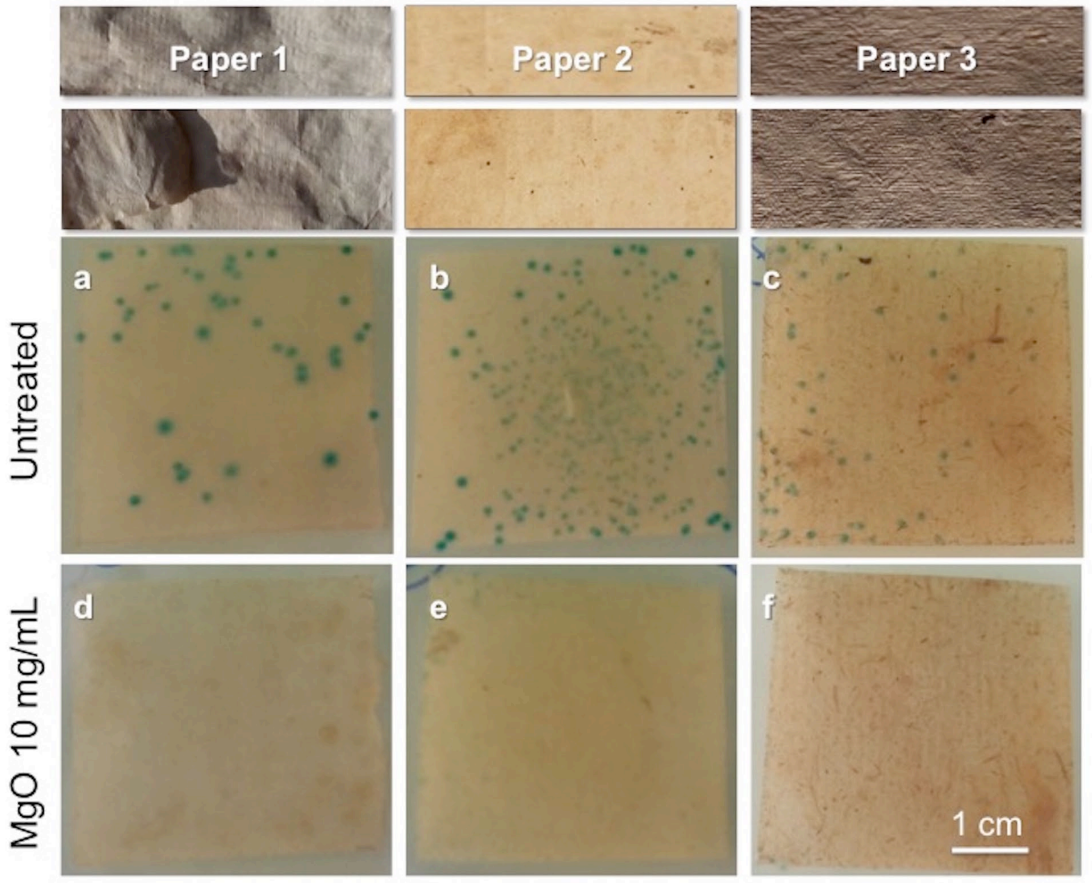

546 **Figure 5.** Images of 18th century papers 1-3 contaminated with *E. coli* and incubated at 37 ºC for 48 h. Panels a-c: untreated papers 1-3; panels d-f: papers 1-3 treated previously with a MgO NP suspension.
548 Blue spots are colonies of *E. coli* stained with a chromogenic compound from TBX agar. Papers 1-3 treated with a suspension of MgO NPs resist *E. coli* colonisation.